

Design charts for linear elastic pavements

Abdullah Fettahoglu, Mehmet Cemal Genes

Online Publication Date: 11 May 2020

URL: <http://www.jresm.org/archive/resm2019.169st1210.html>

DOI: <http://dx.doi.org/10.17515/resm2019.169st1210>

Journal Abbreviation: *Res. Eng. Struct. Mater.*

To cite this article

Fettahoglu A, Genes MC. Design charts for linear elastic pavements. *Res. Eng. Struct. Mater.*, 2020; 6(4): 385-409.

Disclaimer

All the opinions and statements expressed in the papers are on the responsibility of author(s) and are not to be regarded as those of the journal of Research on Engineering Structures and Materials (RESM) organization or related parties. The publishers make no warranty, explicit or implied, or make any representation with respect to the contents of any article will be complete or accurate or up to date. The accuracy of any instructions, equations, or other information should be independently verified. The publisher and related parties shall not be liable for any loss, actions, claims, proceedings, demand or costs or damages whatsoever or howsoever caused arising directly or indirectly in connection with use of the information given in the journal or related means.



Published articles are freely available to users under the terms of Creative Commons Attribution - NonCommercial 4.0 International Public License, as currently displayed at [here](http://creativecommons.org/licenses/by-nc/4.0/) (the "CC BY - NC").



Research Article

Design charts for linear elastic pavements

Abdullah Fettahoglu*^{1,a}, Mehmet Cemal Genes^{2,b}

¹Department of Civil Engineering, Usak University, Usak, Turkey.

²Department of Civil Engineering, Eastern Mediterranean University, Famagusta, Northern Cyprus Turkish Republic

Article Info

Article history:

Received 10 Dec 2019

Revised 24 Apr 2020

Accepted 05 May 2020

Keywords:

Linear elastic pavements;
Design charts;
Hand calculations;
Concrete pavements

Abstract

Deformation of most pavements is practically inelastic. Thus, the exact calculation of pavement deformation often requires use of a damage evaluation law to characterize the stress-strain relationship mathematically. Asphalt, polymer, and reinforced concrete are all examples of such pavements. However, concrete pavements without reinforcement are generally assumed to behave linear elastic. Concrete pavements without reinforcement are used sometimes as permanent pavements with dowels such as airport apron pavement, but sometimes they are used as temporary pavements during the mobilization or initial phases of new construction projects as well. When used as permanent pavements, their design is performed similar to rigid pavements, which has international acceptance by highway engineers, or by finite element analysis. When used as temporary works during the mobilization phase, or when a road is urgently required on a construction site, their design is often problematic, because advanced highway design or finite element analysis might be momentarily unavailable. A rapid, conservative, and reliable hand calculation method for temporary concrete pavements without reinforcement is therefore required. In this study, design charts are provided to allow hand calculations of temporary concrete pavements. In addition, a numerical example is solved to illustrate the use of derived charts. The effects of certain parameters on the stress behavior of concrete pavements are also investigated.

© 2020 MIM Research Group. All rights reserved.

1. Introduction

In this study, some hand calculation charts are derived to enable quick and conservative design of linear elastic rigid pavements, such as temporary concrete pavements without reinforcement, of the type frequently used at the mobilization phase of construction. The design of a linear elastic rigid pavement is based on the maximum stress developed in the pavement itself and in its base. The source of these stresses relates of course to the heaviest wheel load on the top of the pavement. As a result, the maximum stress develops in the contact zone between the wheel and the pavement. The first stage is therefore the calculation of this maximum (or peak) stress, which is necessary to determine the required strength of pavement. At the same time, the stresses induced by the wheel load are dispersed through the thickness of the pavement, and a reduced, dispersed stress is then obtained at the base of the pavement. The maximum value of these vertical stresses must be less than the bearing capacity of the soil. This leads to the second consideration, which is the calculation of the maximum stress at the pavement base in order to determine the pavement thickness required. Starting from the beginning, Groenendijk (1998), Pottinger (1992), Tielking (1994), De Beer (1996), and Jong (2007) [1-5] investigated the contact stress developed between the wheel and the pavement. Of all, Groenendijk [1] derived formulas to determine the maximum stress between the wheel and the pavement, also referred to as the "Footprint pressure" in the literature. This subject is

*Corresponding author: abdullah.fettahoglu@usak.edu.tr

^a orcid.org/0000-0001-5759-1794; ^b orcid.org/0000-0002-9052-7361

DOI: <https://dx.doi.org/10.17515/resm2019.169st1210>

Res. Eng. Struct. Mat. Vol. 6 Iss. 4 (2020) 385-409

discussed in the first section after the introduction. The issue of the second maximum stress at the base of the pavement is evaluated in the subsequent sections. A 45° stress dispersal in the direction of pavement thickness is generally assumed to calculate that second stress. This assumption is applied in many engineering calculations, and is also supported in the literature [6]. However, it is still unclear whether this proposed 45° stress dispersion and the uniform vertical stress distribution is appropriate. Unfortunately, stress dispersal through pavement thickness is less investigated by the researchers. Among that less data available in the literature, Li et al. [7] investigated the stresses in the pavement for the safety of underground pipelines. They studied a range of parameters in an attempt to reduce the stress in the base of the pavement and in the top of the infrastructure pipe and revealed that the burial depth of the pipes should be increased to provide acceptable levels of stress above the pipes. Therefore, the aim of the present study is to investigate the magnitude and shape of the dispersed wheel load in the pavement base. First, a finite element (FE) model of the pavement and wheel model is developed using ANSYS [8]. Second, pavement is assumed to be linear elastic and wheel is assumed conservatively to be a static load rather than a moving load. Third, the possible parameters that could affect the value and shape of the dispersed load at the pavement base are selected. Fourth, the shape and value of the dispersed load at the pavement base is determined by means of FE analysis. Fifth, verification of the FE model is undertaken using Boussinesq equation. Sixth, the effects of the parameters on the dispersed stress are assessed, and finally design charts are derived to estimate the magnitude and shape of the dispersed stress at the pavement base.

2. Determination of the Contact Stress (First Maximum Stress) between the Wheel and Pavement

Groenendijk [1] performed extensive research on the contact stresses between tyre and pavement. He measured the footprint pressure using the Vehicle-Road Surface Pressure Transducer Array (VRSPATA) system. VRSPATA measures the stresses between relatively slow moving free-rolling tyres and the road surface. It measures the vertical stresses, as well as longitudinal and lateral shear stresses. Groenendijk [1] also performed tests for various combinations of wheel load, tyre inflation pressure, and wheel speed for two wide-base single tyres (type C) [6]. With the VRSPATA system, it is possible to measure stress patterns at the interface between tyre and pavement. Fig. 1 shows an example of a measured 3D stress pattern for a 425/65 R22.5 tyre [6] for an inflation pressure of 0.7 MPa, loaded at 100 kN, moving at 0.3 m/s [5].

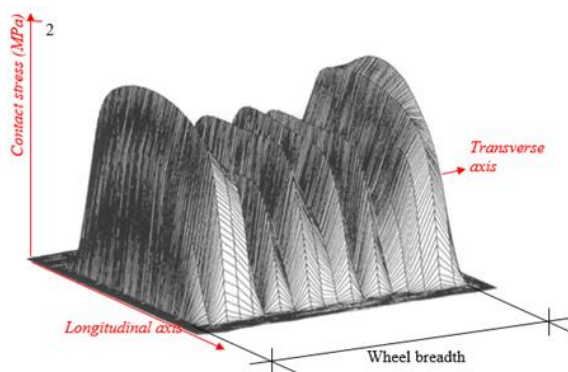


Fig. 1 Example of measuring contact stress using VRSPATA [5].

Groenendijk formulated the following conclusions from his research [5]:

1. The wheel load mainly governs the stresses at the tyre edges, while the tyre pressure governs the stresses at the center of the tyre.
2. The tyre/pavement contact area can be modeled as a rectangle as wide as the tyre tread area, and with a length that depends on the load and inflation pressure. For stress modeling, this area should be divided into three zones in the transverse direction: Two edge zones each 20% of the tyre width, and one middle zone covering the remaining 60%.
3. The vertical contact stresses may be treated as uniformly distributed loads, but generally with different values for the middle and edge zones.

Groenendijk derived equations for the footprint (contact) stress:

$$\sigma_{z,ave,middle} = 422 - 1.20 \cdot F + 4.60 \cdot 10^{-3} \cdot F \cdot p + 0.322 \cdot p + 8.60 \cdot v \quad (1)$$

$$\sigma_{z,ave,edge} = 85.5 + 9.25 \cdot F + 0.290 \cdot p + 1.29 \cdot v \quad (2)$$

where:

F = Wheel load (kN)

p = Tyre inflation pressure (kPa)

v = Wheel speed (m/s)

$\sigma_{z,ave,middle}$ = Average vertical contact stress over the middle 60% of the tyre width (breadth) and the full tyre footprint length (kPa)

$\sigma_{z,ave,edge}$ = Average vertical contact stress over the edges 2 x 20% of the tyre width and the full tyre footprint length (kPa).

Using the load, the inflation pressure, and the velocity, contact stresses can be calculated. The equations derived by Groenendijk are based on measurements for wide-base tyres (type C). It may be assumed that these equations are also valid for the single (type A) and the double (type B) tyres, because these tyre types differ only slightly from the super single (type C) [5]. Fortunately, Jong [5] proved in his thesis that the wheel contact areas given in EC3 [6] are acceptable by means of the Lintrack measurement system used by Jong [5].

If the velocity and tyre pressure in Eq.1 and Eq.2 are conservatively replaced with 0 m/s and 0.9 kPa respectively, Eq.3 and Eq.4 are obtained as follows:

$$\sigma_{z,ave,middle} = 422.3 - 1.2042 \cdot F \quad (3)$$

$$\sigma_{z,ave,edge} = 85.761 + 9.25 \cdot F \quad (4)$$

The variation of contact stresses on edge and middle zones depending on wheel load (N) are given in Fig. 2 using Eq.3 and Eq.4.

Because the method derived here is aimed for the design of temporary concrete pavements, the lowest strength of the pavement can be conservatively taken as 10 MPa (lean concrete). In this case a wheel load or a set of adjacent wheel loads must be 1000 kN to overcome the strength of the concrete and crack the pavement, which is almost impossible in practice. As a result, there is no need to consider the contact stress between the pavement and the wheel in the design of temporary concrete pavements without reinforcement.

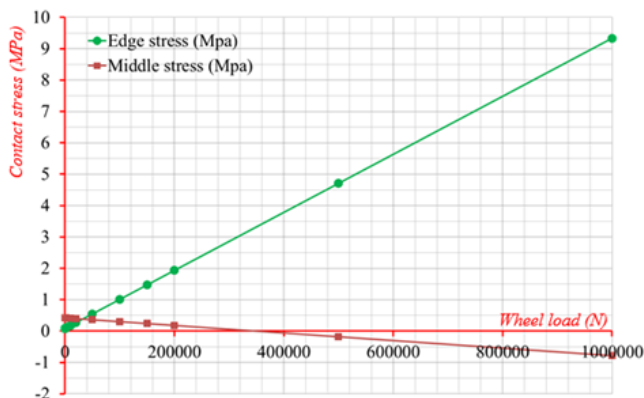


Fig. 2 Variation of edge and middle zone contact stresses according to Eq.3 and Eq.4.

3. Determination of the Dispersed Stress (Second Maximum Stress) at the Pavement Base

The second maximum stress depends on the dispersed stresses at the pavement base, because the wheel-induced stresses might not just be due to a single wheel, but instead, due to a set of wheels. Therefore, it is considered here both the distribution and the maximum of the vertical stress value at the pavement base. If the pavement design is to be performed for more than one wheel, where the wheels are adjacent and interact with each other, the maximum vertical stress can be determined from the superposition of both of the dispersed stresses at the pavement base. To determine the distribution of the dispersed stress at the pavement base, it is first necessary to select the potential parameters influencing the dispersed stress. The effect of these parameters on this distribution is then analyzed separately. Finally, charts are derived for the calculation of the single-wheel load-induced dispersed stress.

3.1. Definition of Parameters

The intended parameters shown in Fig. 3 are *wheel load* (W_L), *wheel breadth* (W_B), *elasticity modulus* (E_P), *Poisson ratio* (ν_P), *width* (W_P) and *thickness of pavement* (T_P). All parameters and their default values are shown in Fig. 3. Finite element (FE) analysis, termed “reference” analysis, is performed using the default (or initial) parameter values. Then, a single parameter is changed, while keeping the others constant. In this way, the effect of this single parameter on the magnitude and distribution of the dispersed stresses is evaluated.

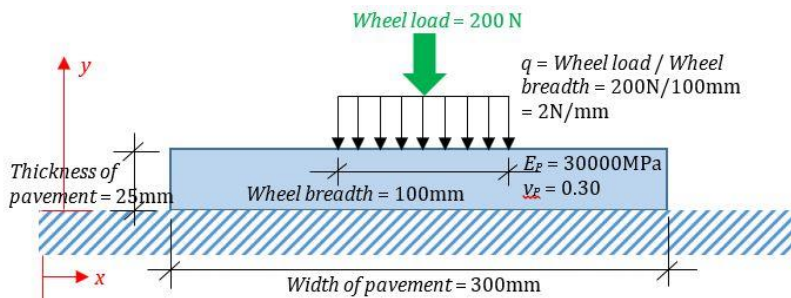


Fig. 3 Default (or initial) values of parameters

3.2. FE Model

The reference FE analysis is used to find the distribution of the dispersed stress at the base of the pavement and additionally in the intermediate layers. The FE model employed in this study is fully restrained against translation and rotation on the pavement base. The number of elements and nodes used in the FE model are 8748 and 9100 respectively. A four-node FE, referred to as SHELL181 in the ANSYS [8] documentation, is used to generate the FE model. Results of the reference FE-analysis, depending on the default values of the parameters are shown in Fig. 4, in which the dispersed stresses (See Fig. 3 for the definitions of the x and y -axes) are given for the top, intermediate, and base layers of pavement. The intermediate layers are selected for various elevations (Values of y in Fig. 4 relate to the y -axis shown in Fig. 3, not the depths of pavement layers).

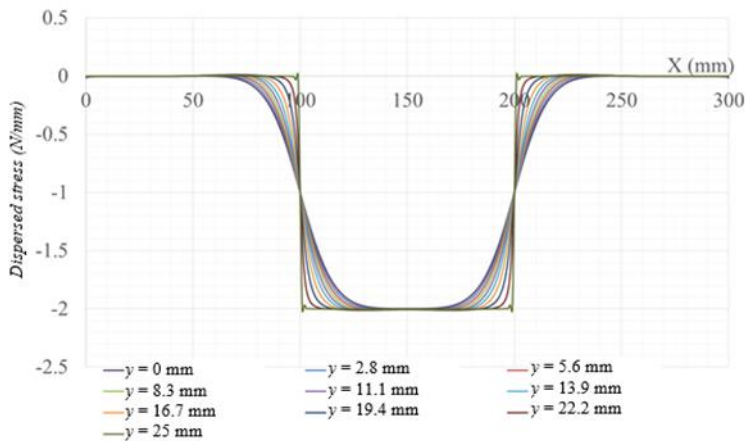


Fig. 4 Dispersed stresses at the top, intermediate layers, and base of pavement.

3.3. Comparison of FE-Analysis with Boussinesq Equation

A comparison of FE-analysis with the Boussinesq equation [9] is performed to determine the dispersed stress at intermediate depths in a semi-infinite continuum (semi-space), as shown in Fig. 5.

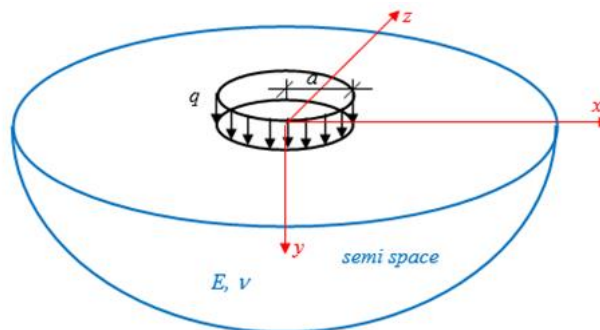


Figure 5. Semi-space with uniform load

The Boussinesq equation for dispersed stress (σ_y) provided by Timoshenko and Goodier [9] is

given below.

$$\sigma_y = q \cdot \left[-1 + \frac{y^3}{(a^2 + y^2)^{1.5}} \right] \tag{5}$$

Using Eq.5 in conjunction with FE results allows comparison between the FE and Boussinesq solutions as shown in Figs. 6a and b.

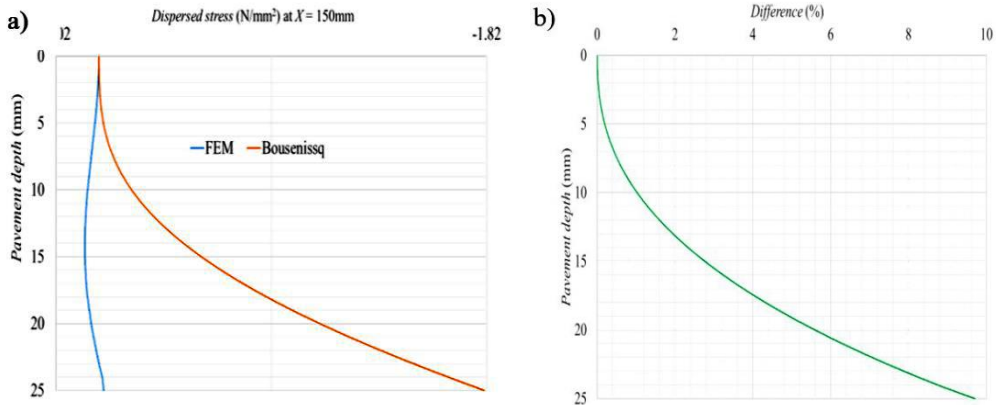


Fig. 6. a) Comparison of FE solution with Boussinesq solution b) Difference (%) between FE solution and Boussinesq solution

The difference between the two solutions is less than 1% up to a depth of 10 mm measured from the top of the pavement. Between 10 mm and almost 20 mm depth, the difference is not more than 5%. The maximum difference is approximately 9.5% at the base of the pavement (25 mm depth). Because the Boussinesq solution is developed for semi-space and results provided by it are more appropriate for small depths, the FE approach used is assumed satisfactory for the intended parameter study.

3.4. Assumed Distribution of Dispersed Load

As seen from Fig. 4 and Fig. 7, the distribution of the dispersed stress at the base of the pavement can be assumed to be trapezoidal, characterized using the dimensions f , e_1 and e_2 given in Fig. 7.

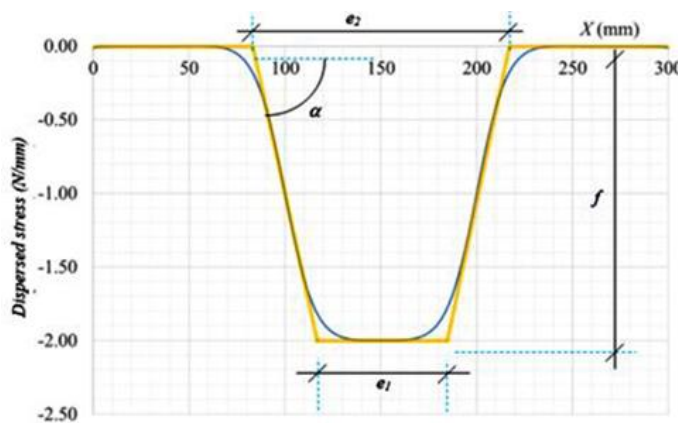


Fig. 7 Distribution of dispersed stress at the pavement base

Here f , e_1 and e_2 are clearly functions of *wheel load*, *wheel breadth*, *elasticity modulus*, *Poisson ratio*, *width*, and *thickness* of pavement. Using the default values of parameters f , e_1 and e_2 results

in -2 N/mm (-1.9979 ≈ -2), 69 mm, and 134 mm respectively, which are derived from Fig. 7 using the Fortran code provided in Appendix 1. The measured value of α is 3.52°. However, f , e_1 and e_2 are not totally independent and the area of the trapezoid must be equal to the wheel load as per Eq.6.

$$\text{Wheel load} = -f \cdot \left(\frac{e_1 + e_2}{2} \right) \tag{6}$$

If Eq.6 is not satisfied, it is advisable to keep f and e_1 the same and justify the value of e_2 , such that Eq.6 holds. In the subsequent sections, f , e_1 and e_2 are obtained as functions of the intended research parameters.

3.5. Effect of Parameters on f , e_1 and e_2

3.5.1 Effect of Elasticity Modulus on f , e_1 and e_2

The elasticity modulus of the pavement (E_p) is varied from 1 GPa to 100 GPa, while other parameter values are kept constant. From the results shown in Fig. 8, it is apparent that f , e_1 and e_2 are independent on the elasticity modulus of the pavement. The values of dispersed stress in Fig. 8 in all scenarios are so same, that all three curves for $E = 1, 10$ and 100 GPa are overlapped.

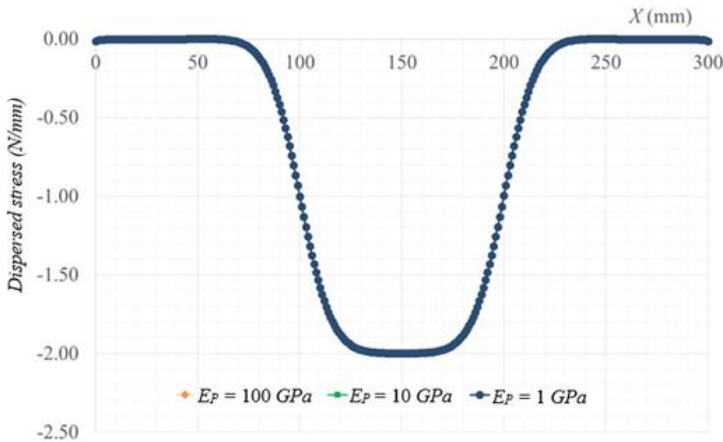


Fig. 8 Dispersed stress at the base of pavement for varying elasticity modulus

3.5.2 Effect of Poisson's Ratio on f , e_1 and e_2

As seen in Fig. 9, the effect of Poisson's ratio on f , e_1 and e_2 is very slight, that it can readily be ignored as a parameter affecting on f , e_1 or e_2 .

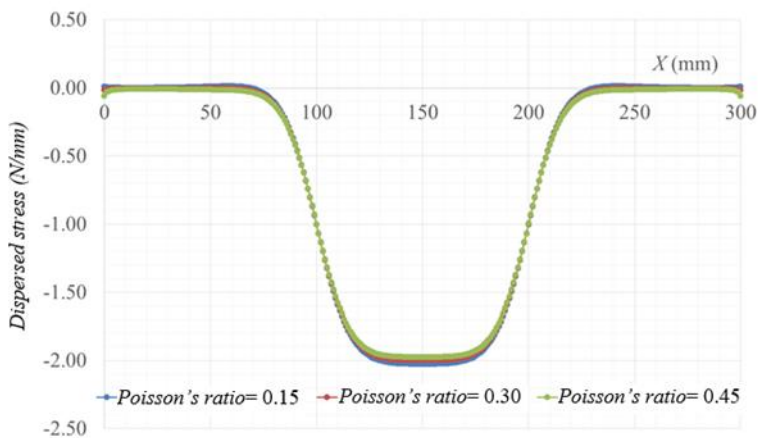


Fig. 9 Dispersed stress at the base of pavement for varying Poisson's ratio.

3.5.3 Effect of Pavement Width on f , e_1 and e_2

The effect of pavement width on f , e_1 and e_2 is shown in Fig. 10. It is clear that widths less than 150 mm lead to stress concentrations at the two edges of the pavement. At the same time, varying the width from 150 mm to 400 mm has almost no effect on the magnitude and distribution of the dispersed stress. Two conclusions may be drawn from Fig. 10: First, the width of the pavement should be at least one and a half times the *wheel breadth* ($Pavement\ width \ge 1.5 \cdot Wheel\ breadth$). Second, varying the width above this value has no effect on f , e_1 and e_2 .

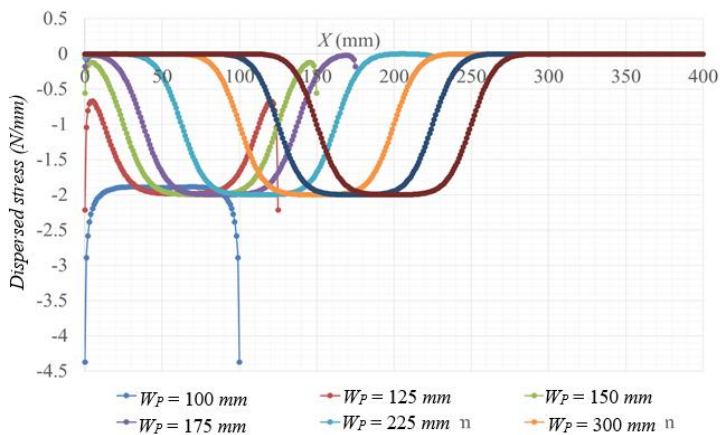


Fig. 10 Dispersed stress depending on the pavement width.

3.5.4 Effect of Wheel Load on f , e_1 and e_2

The variation of the dispersed load depending on wheel load is given in Fig. 11. e_1 and e_2 derived from the curves are all the same, meaning that the wheel load has no effect on them.

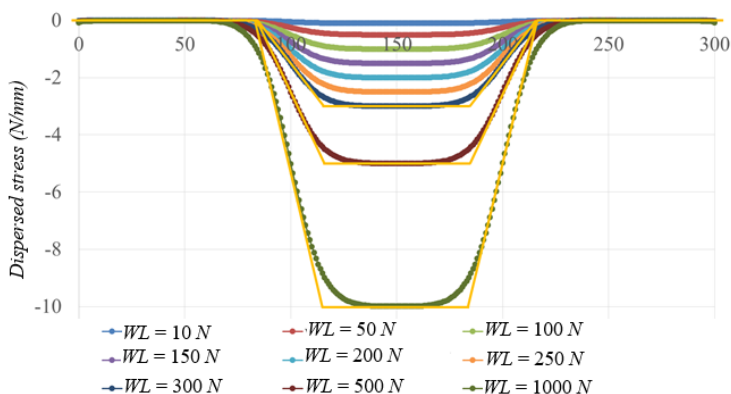


Fig. 11 Dispersed stress depending on the value of wheel load.

Nonetheless, f is directly proportional to the wheel load as given in Fig. 12, if the effect of the remaining parameters (wheel breadth and pavement thickness) are ignored.

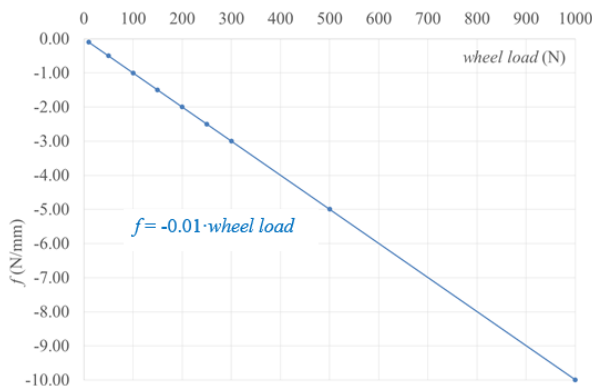


Fig. 12 Variation of f depending on wheel load.

According to Fig. 12, the relationship between f and wheel load is linear and may be described as follows:

$$f = -0.01 \cdot \text{wheel load} \tag{7a}$$

Here, it is apparent that the coefficient (0.01) comes from the ratio, $\text{Wheel Load} / \text{Wheel Breadth}$ for all the cases. For instance, for $W_L = 700$ kN, f derived from Fig. 12 is 7 N/mm, which is equal to 700 N/100 mm = 7 N/mm. As a result, f is described using Eq.7b below.

$$f = -(W_L/W_B) \cdot g(WB, T_P) \tag{7b}$$

where g is a function of wheel breadth and pavement thickness.

3.5.5 Effect of Pavement Thickness on f , e_1 and e_2

As seen in Fig.13, f , e_1 and e_2 , all vary depending on thickness of pavement (T_P).

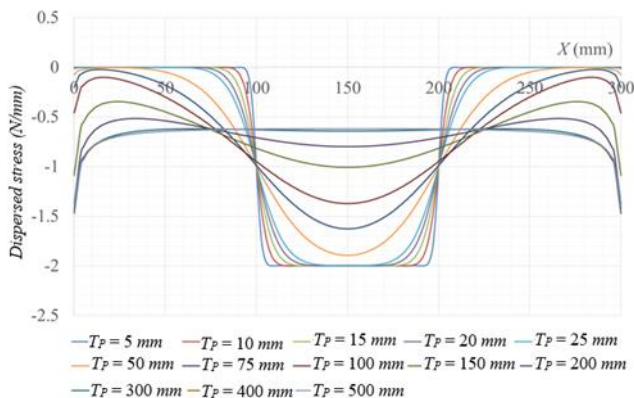


Figure 13. Dispersed stress depending on pavement thickness.

Fig. 13 indicates that starting from a thickness of 75 mm and up to 150 mm, some stress concentrations develop at the edges, but in sufficiently small numbers to allow them to be ignored. However, above a thickness of 150 mm the number of stress concentrations becomes critical, making an applied methodology to derive f , e_1 and e_2 extremely difficult.

3.5.6 Effect of Wheel Breadth on f , e_1 and e_2

Effect of wheel breadth on f , e_1 and e_2 is shown in Fig. 14, from which it is deduced that they are all functions of the parameter *wheel breadth* as in the case of *pavement thickness*.

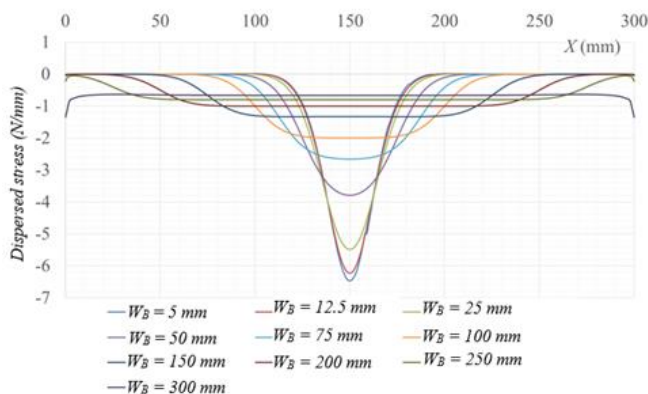


Fig. 14 Dispersed stress depending on *wheel breadth*.

3.5.7 Widening Width of Pavement to Eliminate Stress Concentrations

If the width of pavement is increased to 2 m, the stress concentrations are reduced significantly, however they cannot be completely eliminated especially at extreme pavement thicknesses such as 1000 mm, as observed from Fig. 15. Therefore, the pavement width of 2 m is taken as the default value of the parameter *pavement width* in the FE analyses hereafter. Since the shoulder width in highways is at least 1 m, and half the wheel spacing is approximately 1 m, the default *pavement length* = 1 m + 1 m = 2 m is seen to be realistic.

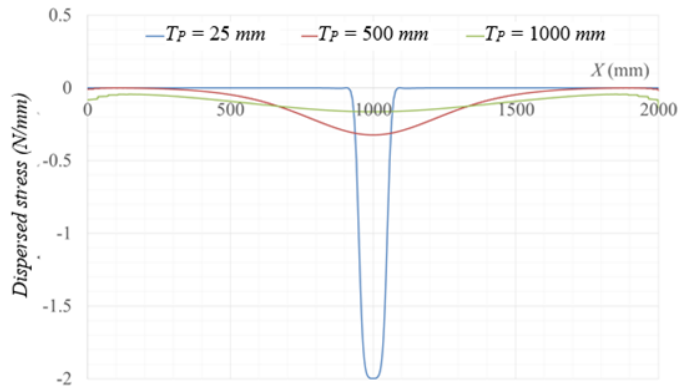


Fig.15 Stress concentrations developed for different pavement thicknesses, when pavement width is 2 m.

3.6. Assumed Distribution of Dispersed Load

Because f depends solely on wheel load, pavement thickness and wheel breadth, the function of f is derived based on these three variables. It has already been shown that f is directly proportional to wheel load according to Eq.7a, the variation of f depending on wheel breadth and pavement thickness for a wheel load of 1 N is shown in the chart given in Fig. 15. Data tables for Figs. 16, 17 and 18 are given in Appendix 2.

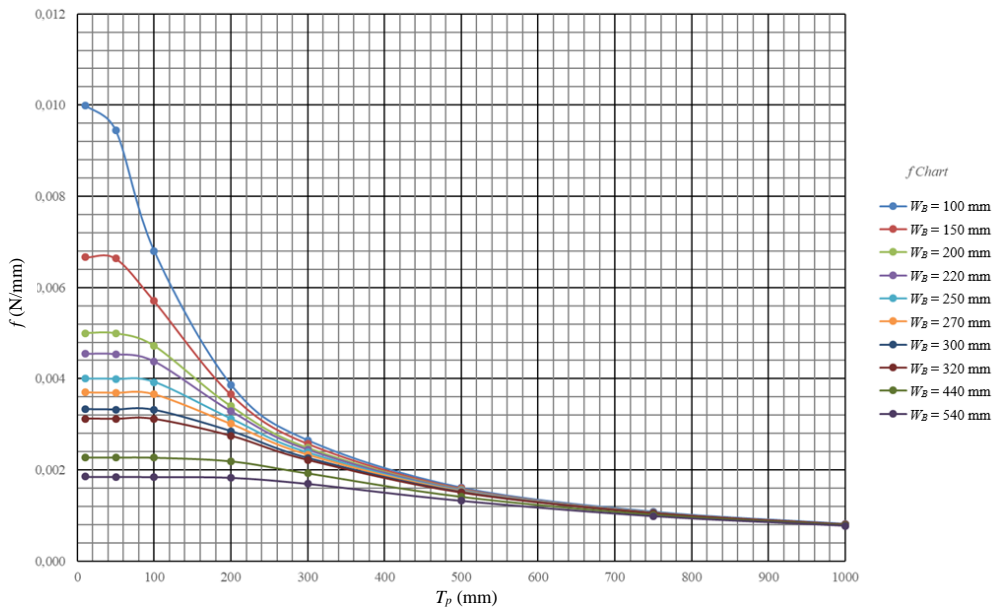


Fig. 16 f depending on pavement thickness (T_P) and wheel breadth (W_B) for wheel load = 1N.

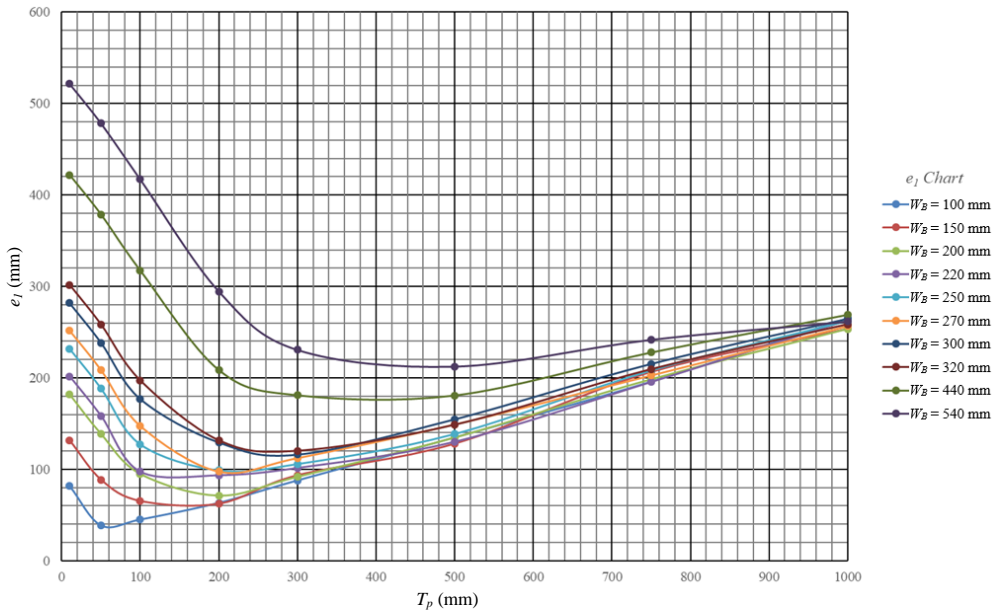


Fig. 17 Recommended values of e_1 .

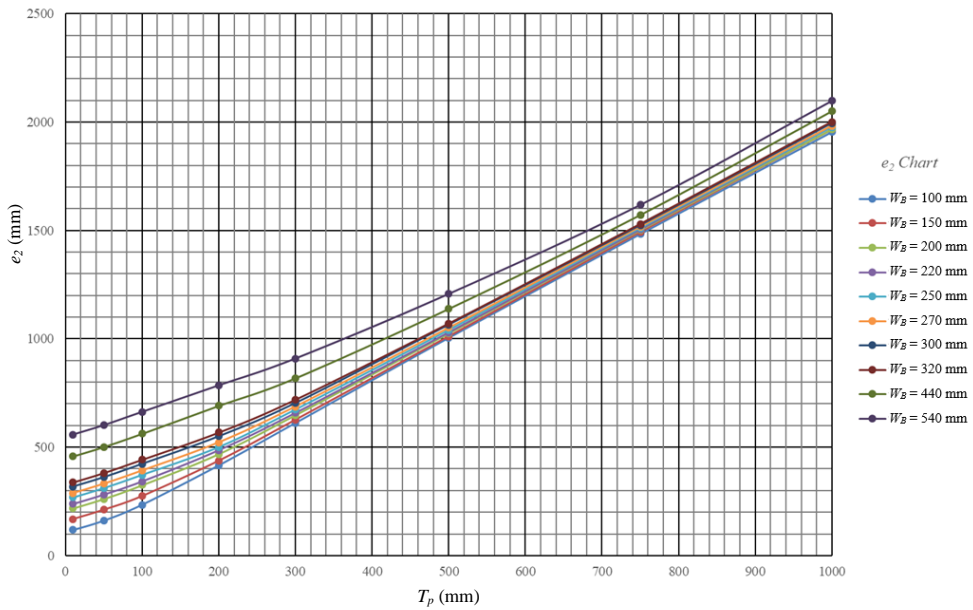


Fig. 18 Recommended values of e_2 .

4. A Numerical Example

The method derived here is a simple hand calculation method for designing concrete (or linear elastic) pavements under axle loads. The method allows rapid and easy calculation of pavement stresses and is especially recommended for engineers unable to perform a FE-analysis due to a lack of time and software. In this section, a truck load is first selected complying with EC 3 [6] and then the magnitude and distribution of stresses developed at the bottom of the pavement are calculated using the charts derived in this study. Finally, results obtained are compared with the results obtained from an FE-analysis.

4.1. Problem Description

According to EC 3 [6] heavy truck vehicles are defined by,

1. Axle number and distance between axles (Table 1, column 1 and 2),
2. Frequently used axle load (Table 1, column 3),
3. Wheel load area and transverse distance between wheel loads (Column 4 of Table 1 and Table 2).

Table 1 Group of frequently used heavy truck vehicles [6].

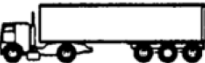
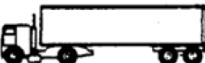
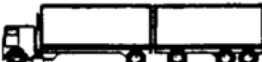
1	2	3	4
<i>View of heavy truck vehicle</i>	<i>Axle distance (m)</i>	<i>Frequently used axle load (kN)</i>	<i>Tyre type</i>
	4.50	90 190	A B
	4.20 1.30	80 140 140	A B B
	3.20 5.20 1.30 1.30	90 180 120 120 120	A B C C C
	3.40 6.00 1.80	90 190 140 140	A B B B
	4.80 3.60 4.40 1.30	90 180 120 110 110	A B C C C

Table 2 Wheel contact areas [6].

<i>Type of wheel area and axle</i>	<i>Geometry</i>
A	<p>Diagram A shows two square wheel contact areas. Each square has a height of 320 mm and a width of 220 mm. The two squares are positioned 2.00 m apart, measured from the center of one square to the center of the other.</p>
B	<p>Diagram B shows two sets of double wheel contact areas. Each set consists of two square contact areas, each 320 mm high and 220 mm wide, spaced 220 mm apart. The two sets are spaced 540 mm apart. The total width of the contact area is 2.00 m.</p>
C	<p>Diagram C shows two square wheel contact areas. Each square has a height of 320 mm and a width of 270 mm. The two squares are positioned 2.00 m apart, measured from the center of one square to the center of the other.</p>

From Table 1, the heavy vehicle in the second row is selected as the truck design load. A C10 concrete pavement without reinforcement is selected. The soil strength is taken as 300 kPa. The thickness of the concrete pavement must be justified to keep the maximum stress at the pavement base lower than the soil strength.

4.2. Solution

The truck loads in the longitudinal and transverse directions are given in Figs. 19, 20, and 21.

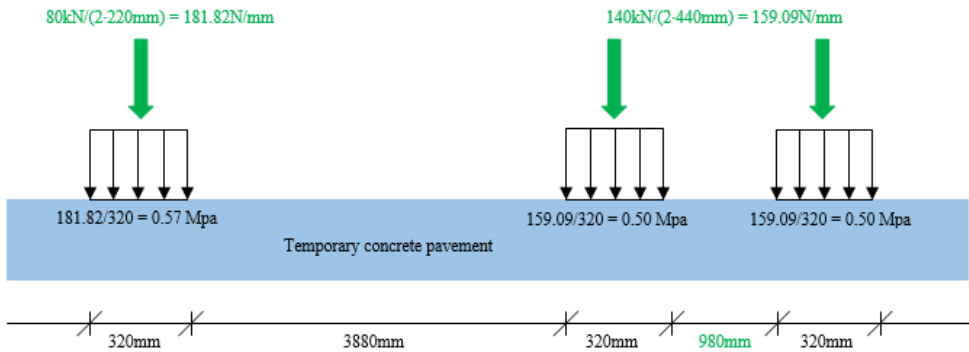


Fig. 19 Truck loading in longitudinal direction.

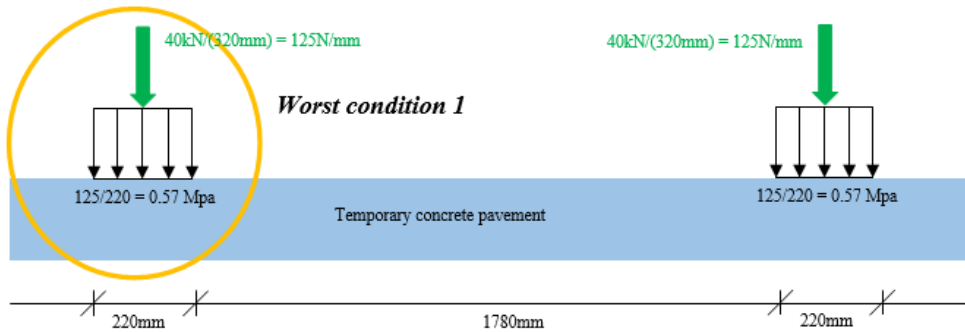


Fig. 20 Truck loading in transverse (1st axle) direction.

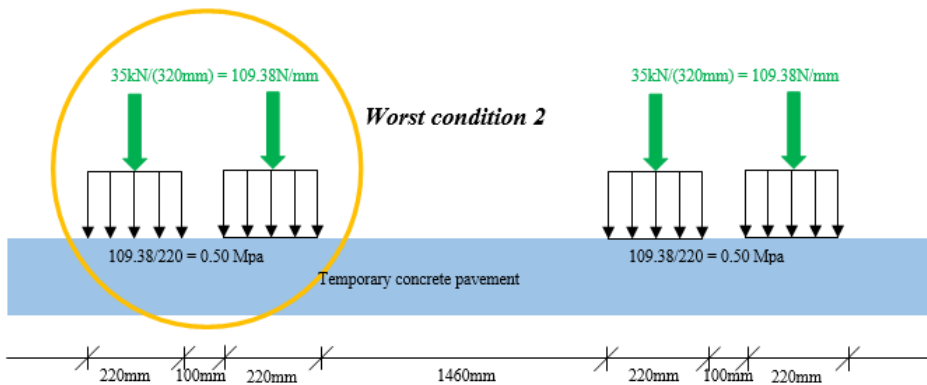


Fig. 21 Truck loading in transverse (2nd or 3rd axle) direction.

4.2.1 Solution of Worst Condition 1

Because the worst condition 1 is composed of a single wheel load, only the maximum stress at the pavement base (f) is calculated, and the shape of dispersed stress (e_1 and e_2) is not required. From Fig. 16, f is determined as follows:

$$125 \cdot f (\text{wheel breadth} = 220 \text{ mm, pavement thickness} = ?) \leq \text{soil strength} = 0.30 \text{ MPa}$$

$$f (\text{wheel breadth} = 220 \text{ mm, pavement thickness} = ?) \leq 0.0024 \text{ MPa}$$

From Figure 16, $f = 0.0022 \text{ MPa} \rightarrow T_p = 320 \text{ mm} = 32 \text{ cm}$

4.2.2 Solution of Worst Condition 2

Because the worst condition 2 is composed of two wheel loads, two maximum stresses at the bottom of the pavement (f) are calculated together with their corresponding distributions (e_1 and e_2 for both). However, since the two wheels are similar, this problem reduces to finding one set of f , e_1 and e_2 and the maximum stress in the interaction zone. From Fig. 16, f is determined as follows:

$$109.38 \cdot f (\text{wheel breadth} = 220 \text{ mm, pavement thickness} = ?) \leq \text{soil strength} = 0.30 \text{ MPa}$$

$$f \leq 0.0027 \text{ MPa}$$

From Fig. 16 $f = 0.0023 \text{ MPa} \rightarrow T_p = 240 \text{ mm} = 24 \text{ cm}$ and

$$109.38 \cdot f = 109.38 \cdot 0.0023 = 0.25 \text{ MPa} \leq \text{soil strength} = 0.30 \text{ MPa}$$

From Fig. 17, e_1 is determined as follows:

$$e_1 (\text{wheel breadth} = 220 \text{ mm, pavement thickness} = 240 \text{ mm}) = 95 \text{ mm}$$

From Fig. 18, e_2 is determined as follows:

$$e_2 (\text{wheel breadth} = 220 \text{ mm, pavement thickness} = 240 \text{ mm}) = 550 \text{ mm}$$

According to these values Fig. 22 is drawn and the maximum stress in the interaction zone is calculated. Using Fig. 22 and the affinity between triangles, this maximum stress is calculated as:

$$2 \cdot 0.0012 \text{ MPa} = 0.0024 \text{ MPa}$$

Since

Max. stress for 1 N = $0.0024 \text{ MPa} < 0.0027 \text{ MPa}$ or,

Max. stress for two adjacent wheel load (Worst condition 2) =

$$= 109.38 \cdot 0.0024 = 0.26 \text{ MPa} < 0.30 \text{ MPa} = \text{Soil strength,}$$

24 cm pavement thickness is enough under selected truck loading.

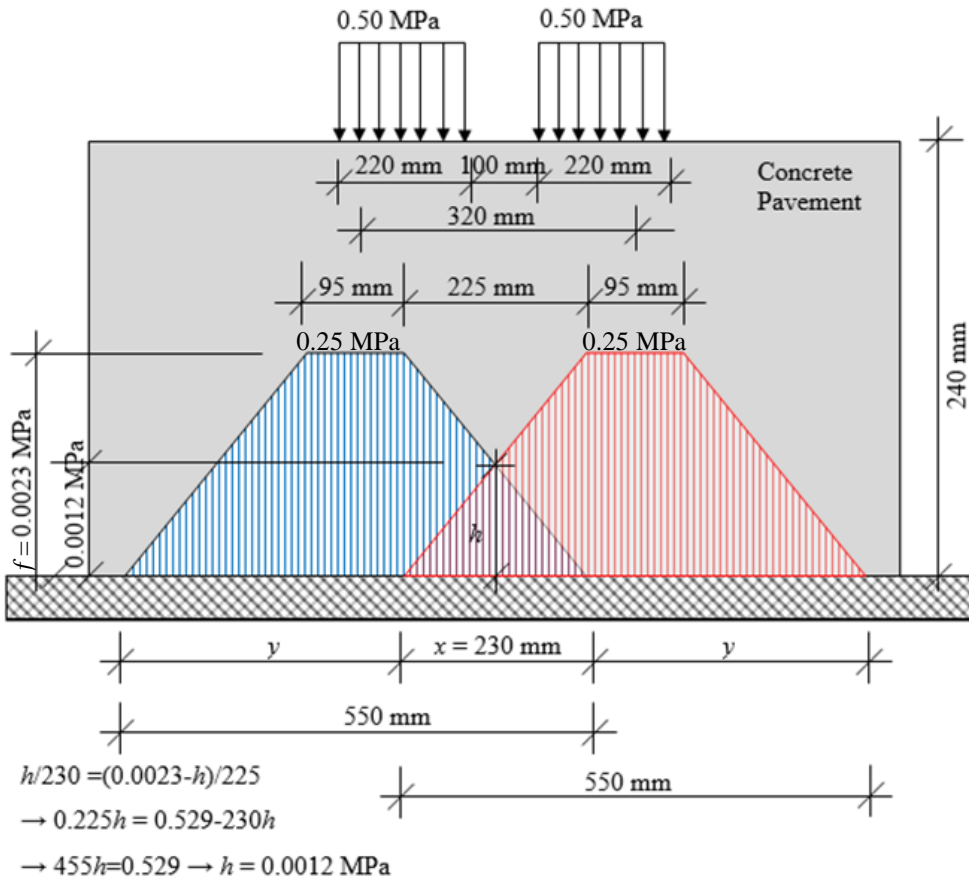


Fig. 22 Interacted dispersed stresses for *pavement thickness* = 24 cm and *wheel breadth* = 220 mm.

5. Conclusion

It is seen that the distribution of dispersed stress can be assumed to be trapezoidal, provided that stress concentrations that may develop at the edges are ignored. The generally assumed 45° angle for stress dispersal is not correct and moreover yields to unsafe pavement thickness values, because the dispersed stress does not remain uniform, but approximately trapezoidal. Thus, the maximum stress developed at the pavement base is aligned with the mid-point of the *wheel breadth*. The *elasticity modulus* and *Poisson's ratio* of the linear elastic pavement have no effect on the stress dispersal. If the *width* of the linear elastic pavement is greater than 1.5 times *wheel breadth*, then the *width* of the linear elastic pavement has also no effect on the stress dispersal. In summary, *f* is a function of *wheel load*, *wheel breadth*, and *thickness of pavement*, while *e₁* and *e₂* are functions of only *wheel breadth* and *pavement thickness*. Charts and tables derived using FE analysis have been verified, and the application of the proposed design method for linear elastic rigid (temporary or permanent concrete) pavements without reinforcement has been explained by means of a numerical example.

References

- [1] Groenendijk, J. Accelerated testing and surface cracking of asphaltic concrete pavement.- (Ph.D. Dissertation, Delft University of Technology, Delft, 1998).
- [2] Pottinger, M.G. The Three-Dimensional Contact Patch Stress Field of Solid and Pneumatic Tires. *Tire Science and Technology*, 1992; 20: 3-32. <https://doi.org/10.2346/1.2139508>
- [3] Tielking, J.K, Abraham, M. A. Measurement of Truck Tire Footprint Pressures. *Journal of the Transportation Research Board*, 1994; 1435: 92-99.
- [4] Beer, M. de. Measurement of tyre/pavement interface stresses under moving wheel loads. *Heavy Vehicle Systems, Special Series, Int. J. of Vehicle Design*, 1996; 3: 97-115.
- [5] Jong, F. B. P. de (2007). Renovation techniques for fatigue cracked orthotropic steel bridge decks.-Ph.D. Dissertation, Delft University of Technology, Delft.
- [6] Eurocode 3 Part 3. Actions on Structures, Brussel, Belgium, 2006.
- [7] Li, Y., Song, G, Cai, J. Mechanical Response Analysis of Airport Flexible Pavement Above Underground Infrastructure Under Moving Wheel Load. *Geotech Geol Eng*, 2017; 35: 2269-2275. <https://doi.org/10.1007/s10706-017-0242-8>
- [8] Swanson Analysis System. ANSYS, USA, 2017.
- [9] Timoshenko, S, Goodier, J. N. *Theory of Elasticity*, McGraw-Hill, New York, USA, 1969.

Appendices

Appendix 1

The Fortran code is given below.

```

IMPLICIT REAL*8 (A-H,O-Z)
CHARACTER*20 DAT,out1
CHARACTER*1 DA(20)
parameter(imax=80000,nmax=2600000)
double precision dp(nmax)
dimension fslp(3)
integer in(imax),nslope
WRITE(*,*)'Name of The Data File'
READ(*,550) DA
OPEN(4,FILE='DNAME')
K=0
DO 1 I=1,20
IF(DA(I).EQ.' ')GO TO 2
1  K=K+1
2  WRITE(4,*)''',(DA(I),I=1,K),''''
   WRITE(4,*)''',(DA(I),I=1,K),'.OUT'''
   REWIND 4
   READ(4,*)DAT
   READ(4,*)out1
   CLOSE(4,STATUS='DELETE')
550 FORMAT(20A1)
   OPEN(5,FILE=DAT)
   OPEN(10,FILE=out1)
C*****
   read(5,*) numdata ! number of data at the curve

c      data1=dp(1)
      i1=1+numdata*2

      call data_read(numdata,dp(1))

c      slope_x=dp(i1)
      i2=i1+3
c slope_x=dp(i2)
      i3=i2+3
c islope_p=in(1)
      n1=1+3

      call max_min(numdata,dp(1),dp(i1),dp(i2),in(1))

      nslope=1
      call slope_cal(numdata,dp(1),dp(i1),dp(i2),in(1),fslp(1))

      call calc_a_b(numdata,dp(1),dp(i1),dp(i2),in(1),fslp(1))
      aa=1.

stop
end

```

```

subroutine calc_a_b(numdata,data1,slope_x,slope_y,islope_p,fslp)
IMPLICIT REAL*8 (A-H,O-Z)
Dimension data1(numdata,2),slope_x(3),slope_y(3),fslp(3)
Integer islope_p(3)

w=slope_y(1)
a=w/atan(fslp(1))
aA=slope_x(1)-a
  aB=slope_x(1)+a

  x=slope_y(2)
b=w/atan(fslp(2))
bA=slope_x(2)+b
  bB=slope_x(2)-b

  e1=bA-aB
  e2=bB-aA
  f=slope_y(3)

  write(*,*) "e1=",e1
  write(*,*) "e2=",e2
  write(*,*) "f=",f

  write(10,*) "e1=",e1
  write(10,*) "e2=",e2
  write(10,*) "f=",f

return
end

subroutine slope_cal(numdata,data1,slope_x,slope_y,islope_p,fslp)
IMPLICIT REAL*8 (A-H,O-Z)
Dimension data1(numdata,2),slope_x(3),slope_y(3),fslp(3)
Integer islope_p(3),htype

htype=2    ! "1" for h, "2" for 2h

if (htype.EQ.1) then

  do j=1,3

    i=islope_p(j)
    h=data1(i,1)-data1(i-1,1)
    fx_ip2=data1(i+2,2)
    fx_ip1=data1(i+1,2)
    fx_im1=data1(i-1,2)
    fx_im2=data1(i-2,2)
    fslp(j)=(-fx_ip2+8*fx_ip1-8*fx_im1+fx_im2)/(12*h)

  enddo

else

```

```

do j=1,3

    i=islope_p(j)
    h=2*(data1(i,1)-data1(i-1,1))
    fx_ip2=data1(i+4,2)
    fx_ip1=data1(i+2,2)
    fx_im1=data1(i-2,2)
    fx_im2=data1(i-4,2)
    fslp(j)=(-fx_ip2+8*fx_ip1-8*fx_im1+fx_im2)/(12*h)

enddo

endif

return
end

subroutine data_read(numdata,data1)
IMPLICIT REAL*8 (A-H,O-Z)
Dimension data1(numdata,2)

do i=1,numdata
    read(5,*) (data1(i,j), j=1,2)
    data1(i,2)=data1(i,2)*(-1)
enddo

return
end

subroutine max_min(numdata,data1,slope_x,slope_y,islope_p)
IMPLICIT REAL*8 (A-H,O-Z)
Dimension data1(numdata,2),slope_x(3),slope_y(3)
Integer islope_p(3)
amax=0.0
amin=0.0

do i=1,numdata
    if(data1(i,2).GE.amax) then
        amax=data1(i,2)
    endif

    if(data1(i,2).LE.amin) then
        amin=data1(i,2)
    endif

enddo

slope_point=(amax+amin)/2.
error=abs(amax-slope_point)

slope_x1=0.0
slope_y1=slope_point

```

```
do i=1,numdata/2
  adiff=abs(data1(i,2)-slope_point)
  if(adiff.lt.error) then
    error=adiff
slope_x(1)=data1(i,1)
    slope_y(1)=data1(i,2)
    islope_p(1)=i
  endif
enddo

error=abs(amax-slope_point)
do i=numdata/2,numdata
  adiff=abs(data1(i,2)-slope_point)
  if(adiff.lt.error) then
    error=adiff
slope_x(2)=data1(i,1)
    slope_y(2)=data1(i,2)
    islope_p(2)=i
  endif
enddo

slope_x(3)=data1(numdata/2,1)
slope_y(3)=data1(numdata/2,2)
islope_p(3)=numdata/2

!      write(10,*) "slope_point=",slope_point

write(10,*) "slope_x1=",slope_x(1)," slope_y1=",slope_y(1)
write(10,*) "slope_x2=",slope_x(2)," slope_y2=",slope_y(2)
write(10,*) "slope_x3=",slope_x(3)," slope_y3=",slope_y(3)

!      write(*,*) "slope_point=",slope_point

write(*,*) "slope_x1=",slope_x(1)," slope_y1=",slope_y(1)
write(*,*) "slope_x2=",slope_x(2)," slope_y2=",slope_y(2)
write(*,*) "slope_x3=",slope_x(3)," slope_y3=",slope_y(3)

return
end
```

Appendix 2

Data tables for Figs. 16, 17 and 18 are provided below respectively.

Table 3. Data Table (f values) for Fig. 16.

T_p (mm)	$wB=100$ mm	$wB=150$ mm	$wB=200$ mm	$wB=220$ mm	$wB=250$ mm	$wB=270$ mm	$wB=300$ mm	$wB=320$ mm	$wB=440$ mm	$wB=540$ mm
10	0.009996	0.006666	0.005000	0.004545	0.004000	0.003704	0.003333	0.003125	0.002273	0.001852
50	0.009446	0.006637	0.004993	0.004537	0.003990	0.003695	0.003326	0.003119	0.002271	0.001851
100	0.006803	0.005707	0.004720	0.004379	0.003927	0.003664	0.003318	0.003117	0.002268	0.001847
200	0.003870	0.003656	0.003399	0.003290	0.003124	0.003014	0.002852	0.002747	0.002189	0.001831
300	0.002649	0.002579	0.002488	0.002447	0.002382	0.002336	0.002265	0.002217	0.001924	0.001697
500	0.001610	0.001594	0.001573	0.001563	0.001546	0.001534	0.001515	0.001501	0.001409	0.001323
750	0.001081	0.001076	0.001070	0.001067	0.001061	0.001058	0.001051	0.001047	0.001015	0.000984
1000	0.000815	0.000813	0.000810	0.000809	0.000806	0.000805	0.000802	0.000800	0.000786	0.000772

Table 4. Data Table (e_t values) for Fig. 17.

T_p (mm)	$w_B=100$ mm	$w_B=150$ mm	$w_B=200$ mm	$w_B=220$ mm	$w_B=250$ mm	$w_B=270$ mm	$w_B=300$ mm	$w_B=320$ mm	$w_B=440$ mm	$w_B=540$ mm
10	81.8	131.8	181.8	201.8	231.8	251.8	281.8	301.8	421.8	521.8
50	38.6	88.5	138.5	158.4	188.4	208.5	238.4	258.4	378.4	478.4
100	45.1	65.3	94.8	97.5	127.4	147.4	177.0	197.2	317.2	417.1
200	63.4	62.3	71.1	93.6	99.0	97.5	129.6	131.8	208.6	294.6
300	88.0	93.5	91.8	101.6	106.0	112.3	116.4	120.4	181.2	230.8
500	13.0	12.1	134.6	130.2	138.8	149.0	155.0	148.9	180.9	212.6
750	196.1	206.7	198.4	195.4	208.2	202.7	215.5	209.6	227.8	241.9
1000	265.5	253.9	253.5	262.8	262.2	256.6	264.7	258.7	268.9	261.7

Table 5. Data Table (e_2 values) for Fig. 18.

T_p (mm)	$w_B=100$ mm	$w_B=150$ mm	$w_B=200$ mm	$w_B=220$ mm	$w_B=250$ mm	$w_B=270$ mm	$w_B=300$ mm	$w_B=320$ mm	$w_B=440$ mm	$w_B=540$ mm
10	118.2	16,2	218.2	238.2	268.2	288.2	318.2	338.2	458.2	558.2
50	161.4	211.5	261.5	281.6	311.6	331.5	361.6	381.6	501.6	601.6
100	234.9	274.7	325.2	342.5	372.6	392.6	423.0	442.8	562.8	662.9
200	416.6	437.7	468.9	486.4	501.0	522.5	550.4	568.2	691.4	785.4
300	612.0	626.5	648.2	658.4	674.0	687.7	703.6	719.6	818.8	909.2
500	100.0	1011.9	1025.4	1029.8	104.2	1051.0	106.0	1071.1	1139.1	1207.4
750	1483.9	1493.3	1501.6	1504.6	151.8	1517.3	1524.5	1530.4	1572.2	1618.1
1000	1954.5	1966.1	1966.5	1977.2	1977.8	1983.4	1995.3	2001.3	2051.1	2098.3